

# Solving inverse problems with the unfolding program TRUEE: Examples in astroparticle physics

N. Milke<sup>a,\*</sup>, M. Doert<sup>a,\*</sup>, S. Klepser<sup>b</sup>, D. Mazin<sup>b</sup>, V. Blobel<sup>c</sup>, W. Rhode<sup>a</sup>

<sup>a</sup>*Experimentelle Physik 5, Technische Universität Dortmund, 44221 Dortmund, Germany*

<sup>b</sup>*IFAE, Edifici Cn., Campus UAB, E-08193 Bellaterra, Spain*

<sup>c</sup>*Institut für Experimentalphysik, Universität Hamburg, D-22761 Hamburg, Germany*

---

## Abstract

The unfolding program TRUEE is a software package for the numerical solution of inverse problems. The algorithm was first applied in the FORTRAN 77 program *RUN*. *RUN* is an event-based unfolding algorithm which makes use of the Tikhonov regularization. It has been tested and compared to different unfolding applications and stood out with notably stable results and reliable error estimation. TRUEE is a conversion of *RUN* to C++, which works within the powerful ROOT framework. The program has been extended for more user-friendliness and delivers unfolding results which are identical to *RUN*. Beside the simplicity of the installation of the software and the generation of graphics, there are new functions, which facilitate the choice of unfolding parameters and observables for the user.

In this paper, we introduce the new unfolding program and present its performance by applying it to two exemplary data sets from astroparticle

---

\*Corresponding author

*Email addresses:* natalie.milke@udo.edu (N. Milke), marlene.doert@udo.edu (M. Doert)

physics, taken with the MAGIC telescopes and the IceCube neutrino detector, respectively.

*Keywords:* unfolding, astroparticle physics, deconvolution, MAGIC, IceCube

---

## 1 Introduction

2 Solving inverse problems can be described as a method to find the cause  
3 of known consequences. Problems of this kind manifest themselves in a wide  
4 range of research fields such as natural sciences, economics and engineering.  
5 Looking at physics as an exemplary field, inverse problems are among the  
6 fundamental challenges in various areas, for instance particle physics, crys-  
7 tallography or medicine. The particular problems and solutions in this paper  
8 will be presented and described alongside the subject of astroparticle physics.  
9 The nomenclature used here is mainly following [1].

10 The structure of this paper comprises three main sections. First, the class  
11 of inverse problems and the general procedure of unfolding with regulariza-  
12 tion are outlined. In a second section, the new unfolding program TRUEE is  
13 introduced. Subsequently, the first applications of the program in astropar-  
14 ticle physics, namely in the data analysis of the experiments MAGIC and  
15 IceCube, are presented in the third section. We conclude with a summary of  
16 the obtained results and an outlook on further extensions and applications  
17 of the program.

## 18 **1. Inverse problems and unfolding**

19 In general, the distribution  $f(x)$  of a variable  $x$  has to be determined.  
20 However, it is often not possible to measure the value  $x$  directly. Instead,  
21 the detector records  $x$ -correlated variables  $y$ . These signals can be seen as  
22 the mentioned consequences of the causation  $x$ . The goal is to get the best-  
23 possible estimate of the  $f(x)$ -distribution from the measured  $g(y)$ -distribution.  
24 As the measurement in a real experiment is distorted, this is not trivial. A  
25 direct allocation of a value  $x$  to a value  $y$  is not possible, because one  $x$  value  
26 causes different signals with different  $y$  values with certain probabilities. Fur-  
27 thermore, the probability to record a signal at all is usually less than one and  
28 depending on  $x$ , which causes a loss of events. Thus, the transformation of  
29  $x$  to  $y$  is disturbed by a finite resolution and a limited acceptance of a real  
30 detector.

31 In mathematics, this problem can be described by the Fredholm integral  
32 equation [2]

$$g(y) = \int_c^d A(y, x)f(x)dx + b(y), \quad (1)$$

33 where  $g(y)$  is the distribution of the measured observable  $y$  and can in general  
34 be multidimensional. The function  $A(y, x)$  is called the kernel or response  
35 function and includes all effects which occur in a real measurement process.  
36 In most cases, this function is not known exactly and has to be determined  
37 by Monte Carlo (MC) simulations, where the measured and the real distri-  
38 butions are known. The parameters  $c$  and  $d$  are the integration limits of the  
39 range where  $x$  is defined ( $c \leq x \leq d$ ). The function  $b(y)$  is the distribution  
40 of a possible background, which is assumed to be known.

41 In reality the measurement delivers discrete values. Furthermore the han-  
 42 dling by the algorithm requires a numerical description of the distributions.  
 43 Thus, a discretization of all functions is required. The distribution  $f(x)$  can  
 44 be parametrized with the Basis-spline (B-spline) functions  $p_j(x)$  [3] and the  
 45 corresponding coefficients  $a_j$

$$f(x) = \sum_{j=1}^m a_j p_j(x). \quad (2)$$

46 The B-spline functions consist of several polynomials of a low degree. In  
 47 the following cubic B-splines are used. They consist of four polynomials of  
 48 third degree each. The points where adjacent polynomials overlap are called  
 49 knots. At the knot positions a B-spline is continuously differentiable up to the  
 50 second derivative, which is important because the second derivative is used  
 51 for the implemented regularization (see Eq. 8). For equidistant knots, the  
 52 cubic B-splines are bell-shaped. Because of the low degree of the polynomials,  
 53 an interpolation with B-spline functions does not tend to oscillate. By using  
 54 this parametrization, the B-spline functions can be included in the response  
 55 function during the discretization:

$$\begin{aligned} \int_c^d A(y, x) f(x) dx &= \sum_{j=1}^m a_j \left[ \int_c^d A(y, x) p_j(x) dx \right] \\ &= \sum_{j=1}^m a_j A_j(y). \end{aligned} \quad (3)$$

56 By integrating over the  $y$ -intervals, the kernel function becomes a response  
 57 matrix:

$$A_{ij} = \int_{y_{i-1}}^{y_i} A_j(y) dy. \quad (4)$$

58 The same integration can be carried out for the measured distribution  $g(y)$   
 59 and the background distribution  $b(y)$ :

$$g_i = \int_{y_{i-1}}^{y_i} g(y)dy, \quad (5)$$

$$b_i = \int_{y_{i-1}}^{y_i} b(y)dy. \quad (6)$$

60 Consequentially, the Fredholm integral equation becomes the matrix equation

$$\mathbf{g} = \mathbf{A}\mathbf{a} + \mathbf{b}, \quad (7)$$

61 with  $\mathbf{g}$ ,  $\mathbf{a}$  and  $\mathbf{b}$  as vectors and  $\mathbf{A}$  as the response matrix. To determine the  
 62 sought distribution  $f(x)$ , the coefficients  $a_j$  need to be found.

63 Solving Eq. 7 is called unfolding and is generally not trivial. Due to the  
 64 finite resolution a smoothing effect on the measured distribution  $\mathbf{g}$  is intro-  
 65 duced. After the rearrangement of the matrix equation this smoothing effect  
 66 is inverted and results in implausible oscillations of the sought distribution  
 67  $f(x)$ . The most straightforward approach for the solution is the inversion  
 68 of the response matrix  $\mathbf{A}$ , if  $\mathbf{A}$  is quadratic and non-singular. The resulting  
 69 inverse matrix  $\mathbf{A}^{-1}$  contains negative non-diagonal elements and very large  
 70 diagonal elements. This causes the mentioned oscillation, which appear in  
 71 any approach of solving Eq. 7 if no additional corrections are applied. This  
 72 is known as a so-called ill-posed problem and generally occurs in all measure-  
 73 ment processes.

74 To suppress the oscillations in the unfolded distribution, so-called regu-  
 75 larization methods are applied. In the presented realization the Tikhonov  
 76 regularization [4] is implemented. The method, in its generalized form, re-  
 77 quires the linear combination of the unfolding term with a regularization term

78 (sometimes called penalty term), which contains a regularization factor. The  
79 regularization term contains an operator, which implies some a-priori as-  
80 sumptions about the solution, such as smoothness. In the current case the  
81 smoothness of the solution is controlled by the curvature operator  $\mathbf{C}$ . A large  
82 curvature corresponds to large oscillations. Thus, reduction of curvature im-  
83 plies reduction of oscillations and that smoothes the resulting distribution.  
84 Since the parametrization of  $f(x)$  is based on cubic B-spline functions, the  
85 curvature  $r(\mathbf{a})$  takes the simple form of a matrix equation

$$r(\mathbf{a}) = \int \left( \frac{d^2 f(x)}{dx^2} \right)^2 dx = \mathbf{a}^T \mathbf{C} \mathbf{a}, \quad (8)$$

86 with  $\mathbf{C}$  as a known, symmetric, positive-semidefinite curvature matrix.

87 The actual unfolding is performed as follows. At first the response matrix  
88  $\mathbf{A}$  is calculated, based on the MC sample. To determine the coefficients  $\mathbf{a}$  of  
89 the final result, the unfolding equation (Eq. 7) is set up, where  $\mathbf{g}$  is the real  
90 measured observable distribution. To fit the right hand side to the left hand  
91 side of this equation, a maximum likelihood fit is performed. For simplicity,  
92 a negative log-likelihood function

$$S(\mathbf{a}) = \sum_i (g_i(\mathbf{a}) - g_{i,m} \ln g_i(\mathbf{a})) \quad (9)$$

93 is formed and minimized. Here  $g_{i,m}$  is the number of measured events in  
94 an interval  $i$  including the possible background contribution in this region.  
95 This number follows the Poisson distribution with mean value  $g_i$ . A Taylor  
96 expansion of the negative log-likelihood function can be written as

$$\begin{aligned} S(\mathbf{a}) &= S(\tilde{\mathbf{a}}) + (\mathbf{a} - \tilde{\mathbf{a}})^T \mathbf{h} \\ &+ \frac{1}{2} (\mathbf{a} - \tilde{\mathbf{a}})^T \mathbf{H} (\mathbf{a} - \tilde{\mathbf{a}}) + \dots, \end{aligned} \quad (10)$$

97 with gradient  $\mathbf{h}$ , Hessian matrix  $\mathbf{H}$  and  $\tilde{\mathbf{a}}$  as a first estimation of coefficients,  
 98 which have to be found.

99 After considering regularization (Eq. 8), the final fit function

$$\begin{aligned}
 R(\mathbf{a}) &= S(\tilde{\mathbf{a}}) + (\mathbf{a} - \tilde{\mathbf{a}})^T \mathbf{h} + \frac{1}{2}(\mathbf{a} - \tilde{\mathbf{a}})^T \mathbf{H}(\mathbf{a} - \tilde{\mathbf{a}}) \\
 &+ \frac{1}{2} \tau \mathbf{a}^T \mathbf{C} \mathbf{a}
 \end{aligned}
 \tag{11}$$

100 has to be minimized to obtain the unfolded result. The regularization pa-  
 101 rameter  $\tau$  controls the effect of the regularization. The challenge is to find  
 102 a proper value for  $\tau$ , to get an optimal estimation of the result as a balance  
 103 between oscillations and the smoothing effect of the regularization.

104 One method to define a value for  $\tau$  is to set up the relation between  $\tau$   
 105 and the effective number of degrees of freedom  $ndf$

$$ndf = \sum_{j=1}^m \frac{1}{1 + \tau S_{jj}}.
 \tag{12}$$

106 Here  $S_{jj}$  are the eigenvalues of the diagonalized curvature matrix  $\mathbf{C}$ , ar-  
 107 ranged in increasing order. The summands in Eq. 12 can be considered as  
 108 filter factors for the coefficients. These coefficients represent the transformed  
 109 measurement and are arranged in decreasing order. The filter factors with  
 110 values  $< 1$  diminish the influence of insignificant coefficients. Accordingly  
 111 an increasing value of  $\tau$  cuts away smoothly the high order coefficients and  
 112 reduces the number of degrees of freedom. In turn, the definition of number  
 113 of degrees of freedom allows the specification of the number of filter factors  
 114 and thus of the regularization strength.

115 To obtain Eq. 12, the Hesse and curvature matrices in Eq. 11 have to be  
 116 diagonalized simultaneously. To do this, a common transformation matrix

117 has to be found, which transforms the Hesse matrix into a unit matrix and  
118 diagonalizes the curvature matrix [5].

119 A lower limit of the parameter  $\tau$  can be estimated by testing the statistical  
120 relevance of the eigenvalues of the response matrix. Applying Eq. 12, the  
121 number of degrees of freedom has to be chosen such that  $\tau$  is above the  
122 suggested limit, in order to avoid the suppression of significant components  
123 in the solution.

## 124 **2. TRUEE**

125 Several algorithms have been developed for solving inverse problems in  
126 different categories. One of them is *RUN* - **R**egularized **U**Nfolding [1] [5],  
127 which uses the mathematics outlined in Sec. 1. *RUN* was developed in  
128 the 1980's in FORTRAN 77 and was updated several times, the last time  
129 around 1995 [6]. The *RUN* algorithm has been converted to a ROOT based  
130 C++ version. Furthermore it has been equipped with additional functions  
131 and user-friendly extensions. This new software package is called TRUEE  
132 - **T**ime-dependent **R**egularized **U**nfolding for **E**conomics and **E**ngineering  
133 problems.

134 The algorithm can process event-wise data input, by reading single n-  
135 tuples of variables. This flexibility permits an individual determination of  
136 the response matrix for every specific case, in contrast to algorithms which  
137 can only deal with histograms as input. Additionally, supplementary cuts  
138 or event weights can be applied internally without changing the input data  
139 files. Furthermore, the availability of individual event information allowed  
140 the development of a method to verify the unfolding result (see Sec. 2.4). A

141 set of up to three observables can be used to perform the unfolding fit. Thus,  
142 the precision of the estimated function can be enhanced by choosing three  
143 observables with complementary information content.

144 *RUN* and TRUEE deliver the same results in terms of both data points  
145 and uncertainty estimation. In Fig. 1 the comparison of the two algorithms  
146 is demonstrated by performing an unfolding of a simulated distribution. The  
147 true distribution and the observable are shown as well, illustrating the finite  
148 resolution and limited acceptance of the simulated measurement. In the  
149 bottom panel, the ratios of the unfolded bin contents show an almost perfect  
150 matching between the algorithms. Minor deviations can be accounted to  
151 the distinct handling of floating point variables of the two different compiler  
152 types.

153 Instead of unfolding a given data sample as a whole, TRUEE can also  
154 be used to investigate changes with time in the investigated distribution. If  
155 structural interruptions with respect to time are found beforehand, TRUEE  
156 can unfold time slices of the inspected data and reveal time-correlated changes  
157 in the corresponding distribution.

158 The installation of TRUEE is straight forward on UNIX based operating  
159 systems, as it uses CMake [7]. The new algorithm is able to deal with two  
160 different types of input files: ASCII and ROOT files. To make the anal-  
161 ysis procedure more comfortable, new functions have been included, which  
162 are described in the following (Sec. 2.1 to 2.3). Besides the newly imple-  
163 mented functionalities, a well-proven *RUN* function for the verification of  
164 the unfolding result shall also be mentioned. The functionalities of a built-in  
165 correction for the acceptance of the experimental setup and the treatment of

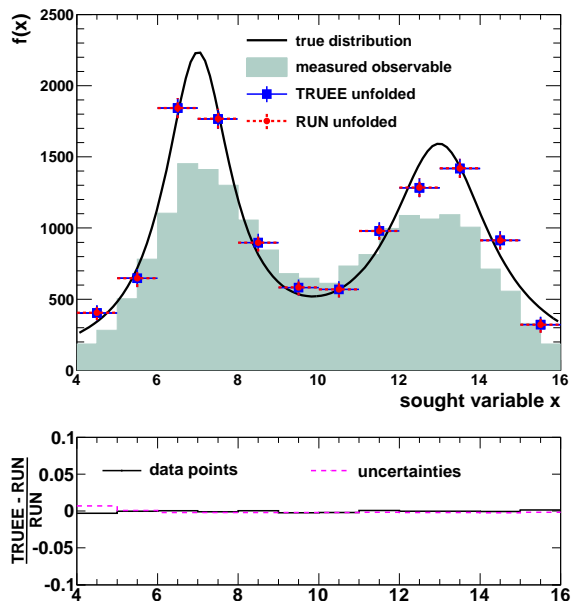


Figure 1: Comparison of results of the original unfolding algorithm  $RUN$  (gray circles) and the new C++ version TRUEE (black squares). The solid line shows the true sought distribution. The shaded area represents the distribution of the measured observable, which has been used for the unfolding. The relative deviations of the bin contents and uncertainties from both algorithms can be seen in the lower figure and show a good agreement between the unfolding results.

166 background that is present in the measurement are likewise inherited from  
 167  $RUN$  and will be described below as well.

168 *2.1. Selection of observables*

169 Generally a measured event is characterized by a large set of observables.  
 170 TRUEE can deal with more than 30 different observables, of which up to  
 171 three can be used for the unfolding at the same time. These should be the  
 172 observables which are most correlated with the variable to be unfolded. To  
 173 check the dependency of the observables on this variable, correlation and

174 profile histograms are automatically created from the MC sample. Different  
175 examples of such histograms are shown in section 3.

## 176 *2.2. Parameter selection*

177 Generally, an unfolding algorithm requires the input of various parameters  
178 by the user, such as the binning of observables and final histogram as well as  
179 the influence of the regularization. The challenge of selecting an optimal pa-  
180 rameter set has its difficulties in finding a result with low correlation between  
181 the unfolded data points and low bias, which is introduced by regularization.  
182 This outcome has to be identified out of many results with different parameter  
183 combinations. The three crucial parameters are

- 184 • number of bins
- 185 • number of knots
- 186 • number of degrees of freedom.

187 The number of knots defines the number of B-splines used in the superpo-  
188 sition for the unfolded function (see Eq. 2). This number is related to the  
189 internal binning of the sought distribution  $f(x)$  for the unfolding, which is  
190 chosen to be equidistant. After the estimation, the obtained  $f(x)$  is trans-  
191 formed to a binned distribution that represents the final result, for which the  
192 number of bins can be chosen. The individual bins can have different widths.

193 The number of degrees of freedom controls the influence of the regular-  
194 ization by defining the parameter  $\tau$  (see Eq. 12). A low number of degrees of  
195 freedom means strong regularization and a positive correlation between the  
196 unfolded data points. Thus, the introduced bias may be too high. A large

197 number reduces the regularization and causes implausibly large fluctuations  
198 and uncertainties. Oftentimes, these can even be larger than the bin contents  
199 due to negative correlations between data points. A balance between these  
200 extreme cases has to be found. In general the number of degrees of freedom  
201 should be roughly the same as the number of bins, as this ensures that on the  
202 one hand no information which is contained in the measurement is discarded  
203 and on the other hand no positive correlations are introduced by solving an  
204 underdetermined system.

205 To facilitate the task of choosing a good combination in the three pa-  
206 rameters outlined above, histograms are provided by TRUEE, which show a  
207 quality value  $\kappa$  that indicates whether the correlations among the unfolded  
208 data points can be neglected. For each number of bins, one such histogram is  
209 provided, where the number of knots and the number of degrees of freedom  
210 are the two dimensions of the histogram. In these histograms, the parameter  
211 region, where the least correlation between the data points can be seen, can  
212 be identified. An example of such a chart is shown in Fig. 2.

213 The displayed correlation-related value  $\kappa$  is the resulting quantity of a test  
214 to determine whether the covariance matrix can be considered as diagonal,  
215 which has been developed within the original algorithm of *RUN*. Within  
216 the test, 5 000 multivariate gaussian deviations of the unfolded result are  
217 randomly generated using the full covariance matrix. Each of the multivariate  
218 deviations is compared to the unfolded result by a  $\chi^2$  calculation, in which  
219 the covariance matrix is assumed to be diagonal. The p-values obtained from  
220 the  $\chi^2$  values are filled into a histogram. In the case of a flat distribution  
221 of p-values the covariance matrix can be considered as diagonal and the

222 correlations between the unfolded data points are negligible. The value  $\kappa$   
 223 describes the flatness of the p-value histogram. It is built as the sum of  
 224 the absolute residuals between the determined and a flat p-value distribution  
 225 divided by the number of bins of the p-value histogram.

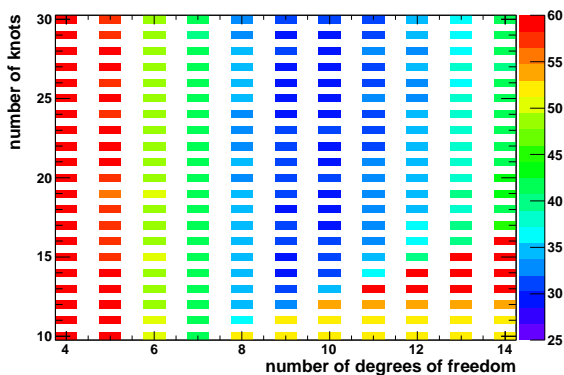


Figure 2: The correlation-related value  $\kappa$ , as a quality factor for the unfolding result, color-coded in the two-dimensional histogram of varying number of knots and number of degrees of freedom. In this example, the best results with the lowest correlations are located in the range between 9 and 11 degrees of freedom. The strong dependency of correlation on the regularization, expressed by the number of degrees of freedom, is clearly visible.

### 226 2.3. Test mode

227 To find an optimal set of unfolding parameters and check whether the  
 228 unfolding is working well with the selected observables, a test mode has  
 229 been implemented as an additional tool. While running in test mode, the  
 230 simulated event sample, which is given to the program, is considered alone. In  
 231 unfolding mode, this sample is only used to determine the detector response  
 232 matrix. In test mode, a fraction of events from the simulated sample can be  
 233 selected to serve as a pseudo data sample, which is subsequently unfolded.

234 The rest of the simulated events is used to determine the response matrix  
 235 in the usual way. Since the true distribution of the variable which is to be  
 236 unfolded is known in a simulation, it is possible to test whether the unfolded  
 237 distribution matches the true one. The comparison between the unfolded and  
 238 the true distributions is performed with a Kolmogorov-Smirnov test [8] and  
 239 a  $\chi^2$  test. Histograms showing the agreement of the distributions for each  
 240 combination of number of knots and degrees of freedom are provided. In test  
 241 mode an additional parameter selection method can be used by plotting  $\kappa$   
 242 versus the values of the  $\chi^2$  test for each parameter set. The parameter sets  
 243 with minimal correlation among the data points and a good fit can be found  
 244 where both the  $\kappa$  and the  $\chi^2$  value are small. An example is given in Fig. 3.  
 245 The parameter setting, which shows the best agreement in the test unfolding,  
 should be used for the actual unfolding of the real data.

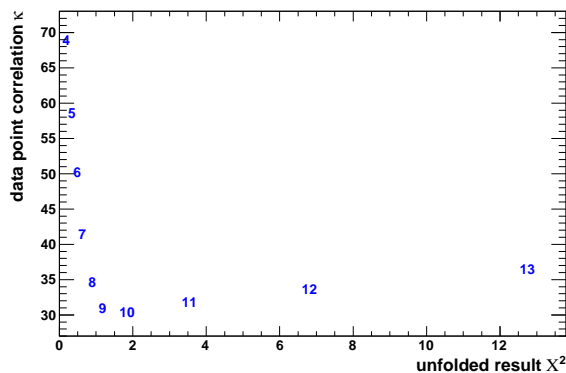


Figure 3: The correlation-related value  $\kappa$  versus the  $\chi^2$  value from the comparison of the unfolded result with the true distribution. The bin contents are marked with the number of degrees of freedom. The optimal result can be found in the region of small  $\kappa$  and small  $\chi^2$  values, here 9 degrees of freedom. The additional variation of numbers of knots and numbers of bins is not shown in this figure.

246

247 *2.4. Verification*

248 Generally, the distributions in detector observables of the MC do not  
249 necessarily match the ones in measured data. After the unfolding result has  
250 been obtained, the consistency of the unfolding and the MC simulation can be  
251 verified by comparing the distributions of individual observables of real data  
252 with a weighted MC sample. To do this, the MC sample, which has been used  
253 to calculate the response matrix, is weighted with respect to the distribution  
254 in the variable  $x$  that is seen in the unfolding result. Hence, following the  
255 same distribution in  $x$ , the resulting MC sample should describe the data  
256 sample perfectly well and all observable distributions should match between  
257 MC and data. This is especially interesting for observables that have not  
258 been considered during the unfolding fit. Histograms showing distributions  
259 of real data and the weighted MC sample are provided for each observable  
260 that has been introduced to the program. Examples are shown in Sec. 3.1.8  
261 and 3.2.5.

262 *2.5. Acceptance Correction*

263 For the reconstruction of the initial distribution  $f(x)$ , which describes the  
264 sought physically meaningful quantity, it is necessary to consider the limited  
265 acceptance and loss of events due to a quality selection during the analysis.  
266 A corresponding correction can be done by TRUEE, if the function of the  
267 generated MC event distribution is supplied by the user. The acceptance of  
268 the measurement, which can be a function of the variable to be unfolded, is  
269 defined as the ratio between the generated MC event distribution and the  
270 MC event distribution at the final analysis level. TRUEE determines this

271 acceptance for each bin of the demanded variable and applies it during the  
272 unfolding of the distribution.

### 273 *2.6. Consideration of background*

274 If background is present in the measurement process, it has to be taken  
275 into account during the unfolding. With a given background event sample,  
276 TRUÉE performs a corresponding correction. By adding the detector observ-  
277 able distributions of the background sample to the expectation (see Eq. 7),  
278 it is considered during the unfolding fit.

## 279 **3. Application of TRUÉE in astroparticle physics experiments**

280 Many ground based astroparticle physics detectors suffer from the fact  
281 that it is not possible to directly measure the primary particles and their  
282 properties. Indirect detection methods are necessary, which instead utilize  
283 atmospheric particle showers or measurements of secondary particles. The  
284 correlation between the distributions in the thus derived observables and  
285 the distribution in the sought quantities is usually complex and ambigu-  
286 ous. Moreover, detection processes are affected by limited acceptance. For  
287 example, the original particle's energy and direction are folded with the in-  
288 teraction cross sections and response of the detector. Thus, the application  
289 of unfolding methods is necessary to determine the distribution of the vari-  
290 able to be found. In this section we present the application of TRUÉE in the  
291 astroparticle experiments MAGIC [9] and IceCube [10].

292 *3.1. The MAGIC telescopes*

293 *3.1.1. The experiment*

294 The **M**ajor **A**tmospheric **G**amma-ray **I**maging **C**herenkov telescopes are  
295 a stereoscopic system of two Cherenkov telescopes, which is situated on the  
296 Roque de los Muchachos on the Canary island of La Palma. MAGIC started  
297 its operation as a single telescope experiment in 2004 and has been upgraded  
298 to a stereoscopic system later on, which is operational since late 2009.

299 The experiment accesses the energy range of 50 GeV to several tens of  
300 TeV in cosmic gamma-rays in the standard operation mode. Measurements  
301 of the gamma-ray flux at these energies give insight into a large set of highly  
302 energetic astronomical sources, such as Supernova Remnants, Active Galactic  
303 Nuclei and potentially Gamma-Ray Bursts. Besides source studies, gamma-  
304 rays also allow the investigation of the extragalactic background light and  
305 more exotic phenomena like the search for dark matter particles.

306 Ground-based gamma-ray detectors like MAGIC exploit the Earth's at-  
307 mosphere as their detection volume. High energy gamma-rays reaching Earth  
308 cause atmospheric particle showers. These are accompanied by Cherenkov  
309 radiation, which can be detected by the telescope cameras. The number of  
310 Cherenkov photons, along with the reconstruction of the shower geometry,  
311 can deliver an energy estimation of each incident gamma-ray.

312 Unfortunately, these events are outnumbered by a huge background of  
313 hadronically induced particle showers, which have to be separated statisti-  
314 cally from the sought gamma particle showers in the course of the so-called  
315 gamma/hadron separation [11],[12],[13].

316 Additional background from diffuse electrons or gamma-rays also influ-

ences the measurement. To determine the size of the remaining background,  
off-source measurements are taken. A convenient way to do this is the so-  
called Wobble observation mode, which permits the simultaneous observa-  
tion of the signal region and a background region [14]. The parameter  $\theta^2$ ,  
which describes the distance in the telescope camera between the expected  
source position and the reconstructed source position for each event, defines  
an “on” region and an “off” region in the camera. This way, the recorded  
background events are taken within the same time as the signal events. It  
is possible to define more than one “off” position, to increase the precision  
of the background measurement. However, to achieve more clarity, only one  
“off” position is used in the application presented here. In this case, the  
determination of the excess between “on” and “off” events can be evaluated  
without further normalization.

### 3.1.2. Spectrum reconstruction procedure

During the analysis of MAGIC data with the analysis package MARS [15],  
the recorded shower images are calibrated, cleaned and characterized by so-  
called image parameters [16]. Among these are the *width* and the *length*,  
describing the root mean square spread of light along and perpendicular to  
the main axis of the image, the light content of the shower (*size*) and the frac-  
tion of light contained in the brightest pixel compared to the total amount of  
light in the image (*concentration*). Some of these parameters are combined  
to the *estimated energy*, using the statistical learning method of Random  
Forest training [17]. This parameter has per construction a very good corre-  
lation with the true energy. Similarly, for the best possible gamma/hadron  
separation, a parameter *hadronness* is built, which describes the probability

342 for each event to be of hadronic origin.

343 To obtain a differential spectrum with respect to the true gamma-ray  
344 energy, an unfolding procedure is applied, using one or several of the ob-  
345 servables at hand. The training of the Random Forests and the unfolding  
346 procedure require Monte Carlo simulated events, which must have undergone  
347 the same analysis procedure up to this point. The simulations used for the  
348 analysis of MAGIC data are produced with the air shower simulation package  
349 CORSIKA [18], followed by the detector simulation [19].

350 At present, the standard MAGIC analysis offers the possibility to per-  
351 form the reconstruction and unfolding procedure in two subsequent steps.  
352 First, data events which contain all formerly mentioned parameters are read  
353 and cuts are applied on *hadronness*, to select gamma-like events, on the sky  
354 coordinates of the recorded events and on  $\theta^2$ , to separate events from the on-  
355 and the off-source measurements. Monte Carlo simulated events are used to  
356 determine the acceptance of the detector, the effective area, and the migra-  
357 tion matrix for the true energy and the observable *estimated energy*. The  
358 product is an energy spectrum of the *estimated energy* and the migration  
359 matrix for the chosen binning.

360 In a second step, different unfolding algorithms with different regulariza-  
361 tion methods can be applied, in order to produce a spectrum with respect  
362 to the true energy [20]. Among the offered regularizations, the methods by  
363 Bertero [21], Schmelling [22] and Tikhonov [4] can be used. The unfolding is  
364 performed using the formerly generated migration matrix. Furthermore, fits  
365 of several functions to the obtained spectrum can be performed, taking into  
366 account the correlation between the unfolded data points.

367 There are several limitations within this procedure. The basis for the  
368 unfolding is fixed to the already binned histogram provided in the first step  
369 of spectral reconstruction. Thus, an optimization of the binning is not pos-  
370 sible during the unfolding process. Furthermore the estimated energy is the  
371 only available observable. Additional observable parameters are not accessi-  
372 ble anymore, but might yield complementary information. The application  
373 of TRUEE offers an alternative approach to the whole reconstruction and  
374 unfolding process, which can avoid these unnecessary limitations.

### 375 *3.1.3. Application of TRUEE*

376 As described in section 2, TRUEE offers the usage of up to three observ-  
377 able parameters for the unfolding. It reads the data sample on event-by-event  
378 basis instead of ready-made histograms, which leaves the program the free-  
379 dom to choose an optimal binning for all the observables. The unfolding  
380 program also performs the acceptance correction of the detector. Moreover,  
381 within the unfolding process, TRUEE can account for the background of  
382 the measurement, using a background event sample. In the standard MARS  
383 analysis this is done prior to the unfolding.

384 The fact that individual events are read by the program requires TRUEE  
385 to enter the analysis process at an earlier step than the current unfolding  
386 tool. This is feasible, as the consideration of the background events does not  
387 need to be carried out before the application of TRUEE. Also, the building  
388 of preliminary histograms is done inside the program during the unfolding  
389 process. Thus, the first step in spectral reconstruction, which has been out-  
390 lined in 3.1.2, is not needed for a TRUEE-based spectrum reconstruction.  
391 Still, the applied cuts as well as the determination of signal and background

392 events are required to be carried out prior to the unfolding. Thus, an inter-  
393 face has been implemented to permit TRUEE to enter the analysis workflow  
394 of the experiment. The tasks which are conducted by this new interface are  
395 outlined in the following.

396 The program reads the events from data and MC simulation files, applies a  
397 cut to exclude hadron-like showers and cuts to choose events which belong to  
398 either the signal or the background region of the telescope camera. It creates  
399 one output file for signal events, one for background events and a third one  
400 for MC events. These files contain all parameters which are relevant for  
401 the unfolding, disengaged from the MAGIC data file tree structure, as even-  
402 level branches. Furthermore, the program reads basic information about the  
403 produced MC events and stores them into an extra tree in the MC file. From  
404 the data sample, the effective observation time is extracted and added to  
405 the signal output file in an additional tree. This additional information are  
406 needed for the acceptance correction which is done within TRUEE as well.

407 After the unfolding process, a script file is used to extract the solution  
408 with the best combination of parameters and to apply a fitting algorithm  
409 which takes into account the correlation between the bins of the unfolded  
410 spectrum. Quoting such a fit result, in addition to the unfolded data points,  
411 is common for the presentation of energy spectra in astroparticle physics,  
412 as it facilitates the comparison of results from different analyses. The cor-  
413 responding fit function can be selected by the user among several choices  
414 (power law, broken power law, etc.).

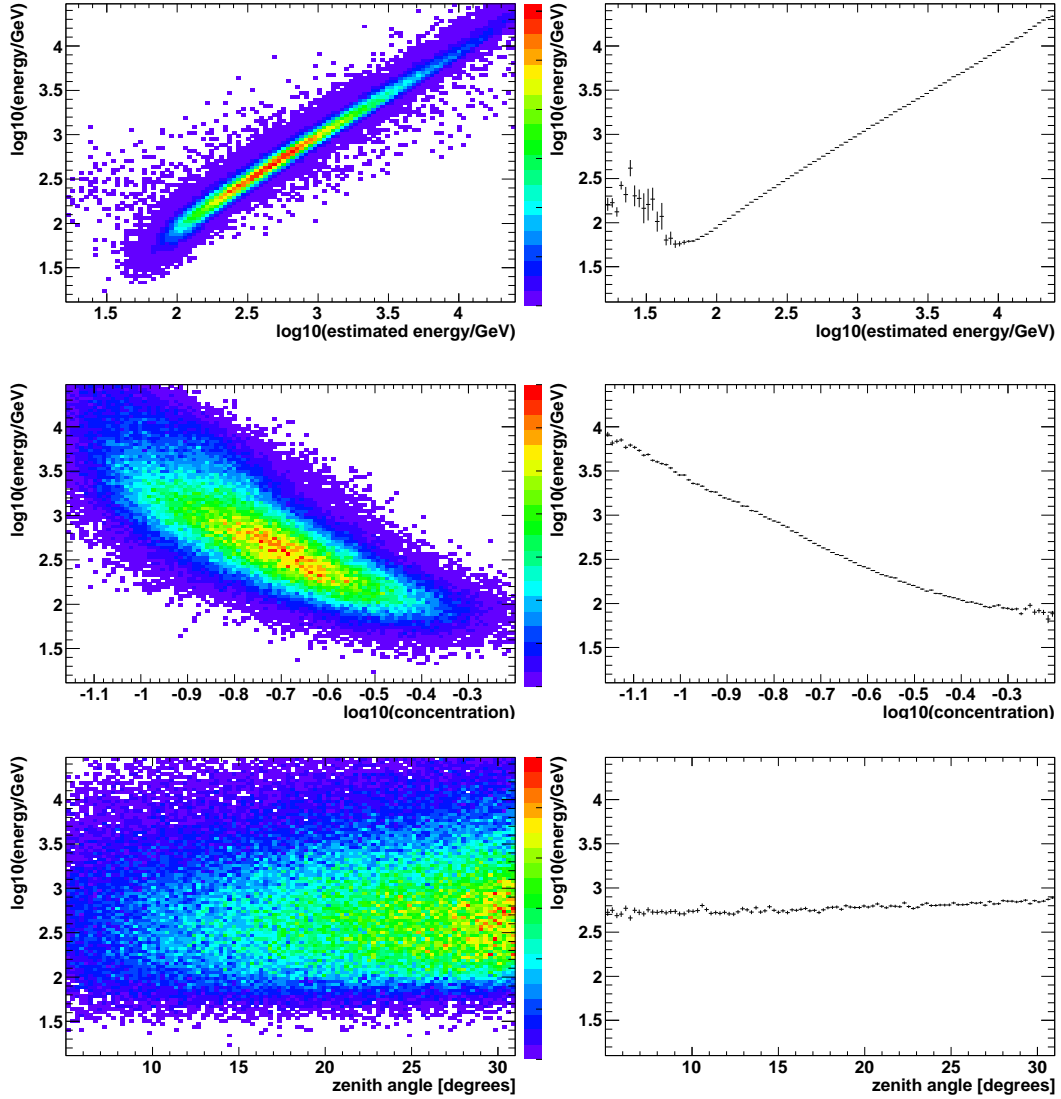


Figure 4: Correlation between the energy and the observational parameters used for the application of TRUEE in the MAGIC analysis. Shown are scatter plots of events (left) and the related profile histograms (right). An optimal correlation is present in a monotonically changing profile function with small uncertainties. The density is displayed in color code.

415 *3.1.4. Choice of observables*

416 For the unfolding of MAGIC data the space of observable parameters has  
417 been investigated. The set of parameters which has proven to deliver good  
418 results are:

- 419 • The *estimated energy*, a combination of observables which is gained  
420 by random forest regression and correlates very well with the true en-  
421 ergy, has been the scaffolding of the current MAGIC unfolding and is  
422 a fruitful contribution also for the unfolding with TRUEE.
- 423 • The parameter *concentration*, which describes the light content ratio  
424 of the brightest pixel compared to the surrounding ones, shows a clear  
425 correlation with the true energy.
- 426 • As a third parameter the *zenith angle* is an important input for an un-  
427 folding with TRUEE. Even though it does not show a good correlation  
428 with the energy, it influences the image of each event in the camera, so  
429 that events with the same energy look different if they have been taken  
430 at different zenith angles.

431 The correlation of each observable parameter with the true energy is shown  
432 in Fig. 4.

433 *3.1.5. Acceptance correction*

434 The data events, which are read by TRUEE, are only those events which  
435 triggered the telescopes and which survived the analysis cuts. Similarly, the  
436 MC set only comprises events which remain after the selection by a simu-  
437 lated trigger and the same analysis cuts. In other words, the measurement

438 is affected by a loss of events compared to the initially arriving particles.  
 439 The ratio between the distributions of the surviving and the arriving parti-  
 440 cles is given by the acceptance of the measurement process. As explained in  
 441 2.5, TRUUEE can deduce this acceptance and apply an appropriate correction  
 442 during the unfolding, in order to get the true distribution in the sought quan-  
 443 tity. For MAGIC data, this generally is the differential flux of gamma-ray  
 444 particles, i.e. the number of particles per unit area, time and energy. Thus,  
 445 the distribution of the MC has to be expressed in the same way. The area in  
 446 which the MC events are generated is given by a circle whose radius is the  
 447 so-called *maximum impact parameter*  $r$ . As MC events do not have a density  
 448 in time, this factor has to be determined by the following consideration. To  
 449 obtain the actual factor between the number of data events collected within  
 450 the actual observation time and the initial flux from the simulations, MC  
 451 and data events have to be related to each other. For this reason the MC  
 452 distribution is normalized to the effective observation time  $T_{obs}$  which the  
 453 real data sample was collected in.

454 Adding this information, the normalization constant of the MC distribu-  
 455 tion can be obtained from the number of generated particles  $N_{gen}$ , the energy  
 456 range which has been simulated ( $E_{min}$  to  $E_{max}$ ) and the spectral index  $\gamma$ ,  
 457 using

$$\frac{d^3 N}{dE dA dt} = C \cdot \left( \frac{E}{1 GeV} \right)^{-\gamma}. \quad (13)$$

458 Integrating yields the number of generated events,

$$N_{gen} = \int_{E_{min}}^{E_{max}} \int_A \int_{T_{obs}} \frac{d^3 N}{dE dA dt} dE dA dt, \quad (14)$$

459 which implies that

$$C = \frac{N_{gen}}{r^2 \cdot \pi \cdot T_{obs}} \cdot \frac{(-\gamma + 1)}{\left(\frac{E_{max}}{1 GeV}\right)^{-\gamma+1} - \left(\frac{E_{min}}{1 GeV}\right)^{-\gamma+1}}. \quad (15)$$

460 In the case of unfolding a MC sample, the flux of particles per time is not  
 461 a meaningful parameter, as neither the auxiliary MC sample nor the target  
 462 sample have such a time density information. So in that case, a distribution  
 463 of particles per area and energy is used.

### 464 3.1.6. Unfolding of MC spectra

465 The unfolding of MC data is presented in several steps. First, a test  
 466 unfolding is performed. In a second step, a different MC sample is used  
 467 as pseudo data. These unfolding procedures handle only the distribution of  
 468 events which remain after the trigger simulation and cuts set during the anal-  
 469 ysis. Subsequently, two examples of an unfolding with an applied correction  
 470 for the acceptance of the detector is shown, which results in a differential flux  
 471 spectrum, i.e. in the case of MC the initial number of particles per energy  
 472 and area which have been generated in the MC simulation. The used MC  
 473 samples are summarized in Tab. 1. The features specified there are the spec-  
 474 tral index of the generated power law distribution, the range in zenith angle  
 475 which is covered by the simulated events and the *maximum impact parameter*  
 476  $r$ , which specifies the area over which the generated events are distributed.  
 477 Furthermore the number of primarily generated events is given as well as the  
 478 number of events which survive after triggers and analysis cuts.

479 Following the above scheme, first of all a test unfolding is performed, using  
 480 only MC sample A. 10 % of the MC is taken as pseudo data to be unfolded,

MC Sample	A	B	C
Spectral index $\gamma$	1.6	2.6	2.6
Zenith angle range	5° - 35°	5° - 35°	5° - 35°
Impact parameter	350 m	350 m	350 m
No. generated	7 893 000	10 000 000	40 000 000
No. residual	272 283	24 444	100 224

Table 1: Summary of the Monte Carlo samples which are used during the unfolding of MAGIC Monte Carlo and data events.

481 and 90 % are used for the response matrix and acceptance calculation. A  
482 wide range of unfolding parameters is probed and the combination which de-  
483 livers the smallest inter-bin-correlation is chosen. For the analysis presented  
484 here, which results in a spectrum with 16 bins, these are 21 knots and 13  
485 degrees of freedom. The resulting MC spectrum can be seen in Fig. 5, where  
486 additionally the true distribution of events is shown. This direct comparison  
487 of the unfolded and the true distribution permits to verify the goodness of  
488 the choice of the used unfolding parameters.

489 A successful test unfolding delivers a good reproduction of the input spec-  
490 trum and information about which parameter combinations give reliable re-  
491 sults. However, in this case the MC and the pseudo data events follow the  
492 same distribution as they stem from the same MC sample. As the simulated  
493 and the real distribution of the data are in general not equal, the performance  
494 for different distributions in MC and pseudo data needs to be investigated.  
495 For this purpose a second MC unfolding is carried out, this time applying  
496 MC sample B as pseudo data, while the whole sample A is used to calculate  
497 the response matrix. The two MC sets show different distributions in energy,

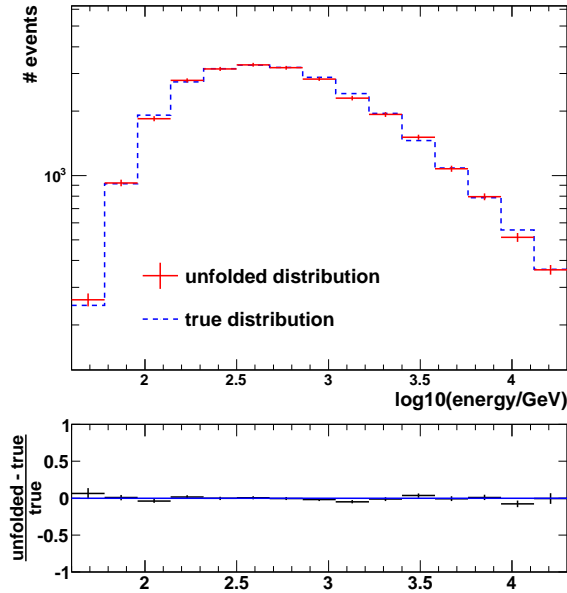


Figure 5: Event distribution obtained with an unfolding of MC events in TRUEE’s test mode. The unfolding result (red points with error bars) is compared to the true distribution known from the MC (blue/dashed curve).

498 such that the spectral indices differ by 1.0. The number of generated events  
 499 in sample B is higher, but due to the steeper spectrum and the decrease of  
 500 the trigger efficiency towards low energies, the final sample is one order of  
 501 magnitude smaller than MC sample A. The ratio of events between data and  
 502 MC events of  $\sim 10$  is also desirable for the unfolding of real data.

503 The unfolding process is carried out with the same binning of observable  
 504 parameters and combinations of unfolding parameters as the test unfolding  
 505 shown above. The result can be seen in Fig. 6.

506 After the unfolding of triggered event distributions, the unfolding of a MC  
 507 sample with applied acceptance correction will be shown. For this purpose,  
 508 MC sample B serves as pseudo data again, while sample A forms the MC

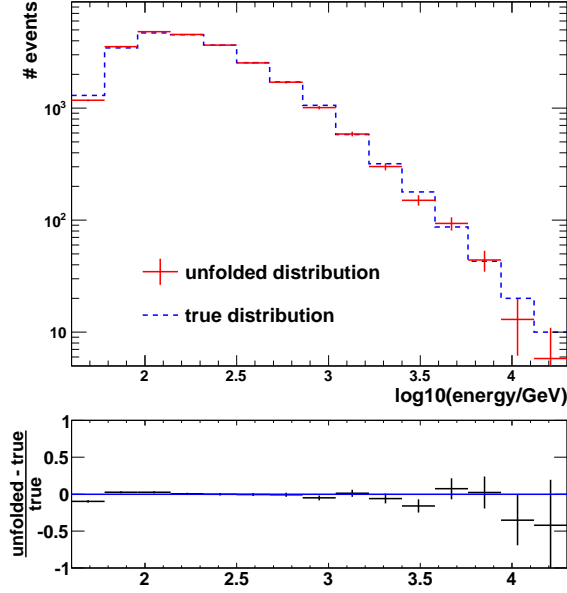


Figure 6: Unfolded event spectrum of MC events. MC sample B with spectral index  $\gamma_B = 2.6$  has been unfolded as pseudo data, applying MC sample A with spectral index  $\gamma_A = 1.6$ . The unfolded points of the event spectrum (red points with error bars) and the original distribution (blue/dashed curve) are shown.

509 sample for the determination of the response matrix. Additionally, the initial  
 510 distribution of sample A is given as

$$\frac{d^2 N}{dE dA} = \frac{N_{gen}}{r^2 \cdot \pi} \cdot (-\gamma + 1) \cdot \frac{\frac{E}{1 \text{ GeV}}^{-\gamma}}{\left(\frac{E_{max}}{1 \text{ GeV}}\right)^{-\gamma+1} - \left(\frac{E_{min}}{1 \text{ GeV}}\right)^{-\gamma+1}}, \quad (16)$$

511 with  $E_{min} = 10 \text{ GeV}$  and  $E_{max} = 30\,000 \text{ GeV}$ . For the remaining quantities  
 512 see Tab. 1.

513 The unfolding itself is performed with the same binning of the observables  
 514 and with the same unfolding parameters. Figure 7 shows the unfolded dis-  
 515 tribution and the initial MC function. It has to be noted that, while a good

516 agreement is achieved at intermediate energies, the distribution at lower en-  
517 ergies appears to be systematically underestimated. This effect is caused by  
518 the fact that the acceptance correction refers to the center of gravity within  
519 each bin of the initial MC distribution. For large differences between the  
520 spectrum of the MC sample used to determine the response matrix and of  
521 the spectrum obtained by the unfolding procedure, the relative shift between  
522 the centers of gravity of the two distributions is not negligible anymore.  
523 However, this effect can be corrected, if - in the case of such discrepancies in  
524 the spectra - a second step of unfolding with acceptance correction is applied,  
525 using a re-weighted MC spectrum which is more similar to the result of the  
526 first step.

527 For the study presented here, the unfolding of the pseudo data sample  
528 with acceptance correction is repeated using MC sample C (see Tab. 1),  
529 which shows the same spectral index as the pseudo data. The result can be  
530 seen in Fig. 8. Obviously, the formerly seen discrepancies at low energies do  
531 not appear in this case.

532 Still, the unfolding itself is only slightly affected by this dependency. It  
533 delivers good results for the event spectra, also for this significant difference in  
534 the spectral indices, as can be seen in the Fig. 6. The remaining discrepancy  
535 at very low energies disappears after the above mentioned correction.

### 536 *3.1.7. Unfolding of a MAGIC data sample*

537 After the successful application of TRUEE in the MAGIC unfolding of  
538 MC spectra, a proof of principle on real telescope data is given in the fol-  
539 lowing. For this purpose the standard candle of gamma-ray astronomy, the  
540 Crab Nebula, serves as an exemplary source. A test data sample which is

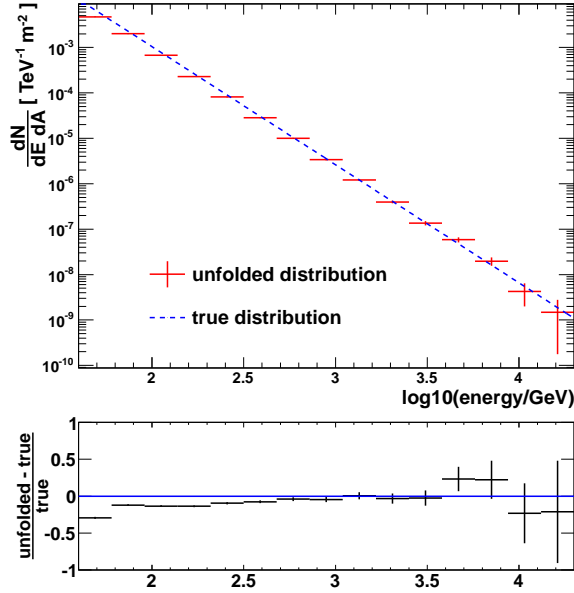


Figure 7: Unfolding of MC simulations as pseudo data with built-in acceptance correction of TRUÉE. MC sample B is unfolded as pseudo data, while MC sample A serves as MC in the unfolding. The red points with error bars represent the result of the unfolding. The blue solid line shows the true initial MC distribution.

541 described below is analyzed with both the standard MAGIC analysis chain  
 542 and the new chain including TRUÉE. Finally a comparison of the results  
 543 is shown. We would like to state at this point that the presented analysis  
 544 is not optimized for extracting any results regarding the physics of the ob-  
 545 served source or the telescope performance. It only serves as an example  
 546 of the compatibility of the two analyses. Studies on the performance of the  
 547 MAGIC stereo system can be found in [9].

548 The data sample comprises 7.3 hours of Crab Nebula observations taken  
 549 with the MAGIC telescopes. The data have been taken in Wobble observa-  
 550 tion mode.

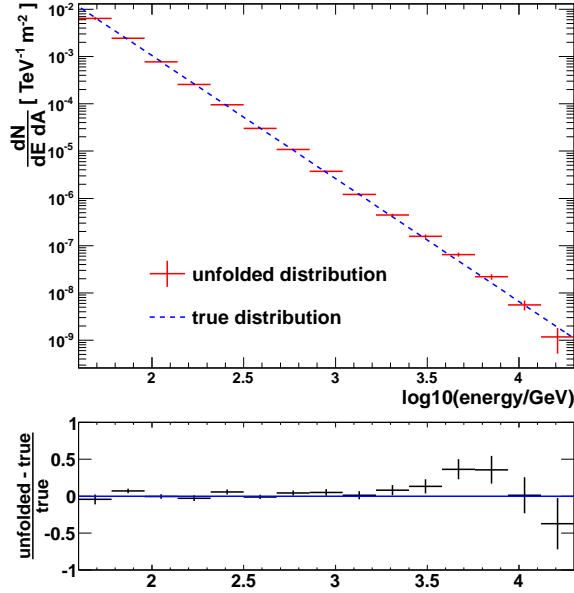


Figure 8: Unfolding of MC simulations as pseudo data with built-in acceptance correction of TRUEE. Unlike in Fig. 7, the pseudo data sample MC B is unfolded using MC sample C, which features the same spectral slope. The result of the unfolding is given by red points with error bars. The blue solid line represents the true initial MC distribution.

551 The preparation of the data, including the conversion of the extracted  
 552 charge into the number of photons at the photodetector, the cleaning of  
 553 the shower images and the determination of image parameters to the light  
 554 distributions are identical for both analyses. The standard MAGIC analysis  
 555 and the TRUEE-based analysis diverge at the point where both the data and  
 556 the MC are preprocessed such that the events are all characterized by image  
 557 parameters and are assigned an *estimated energy* and a *hadronness*.

558 In the current MAGIC analysis, a standard analysis following [9] has been  
 559 used to derive cuts for the separation of gammas and hadrons and for the  
 560 determination of the “on” and the “off” event sample, using the standard

561 spectrum reconstruction tool. The obtained cuts are applied on the MC and  
562 on the data sample. MC sample A is used to determine the effective area of  
563 the measurement and to build the migration matrix. The resulting spectrum  
564 of differential flux vs. estimated energy is unfolded using the current MAGIC  
565 tool and the generated migration matrix. Several executions with different  
566 regularization methods have been performed, leading to compatible results.

567 Following the analysis chain presented in this paper, the event files are  
568 processed by the aforementioned interface. The applied analysis cuts are the  
569 same as the ones used in the standard MAGIC analysis example. TRUEE  
570 is performed using also MC sample A to calculate the migration matrix and  
571 to obtain the overall acceptance. Events which are sorted into the off-source  
572 measurement sample are given to TRUEE as background events. For the case  
573 of one “off” region, no normalization in terms of weighting has to be applied  
574 to these events as in Wobble mode, the on- and off-source measurements  
575 are taken simultaneously. The chosen set of unfolding parameters, namely  
576 number of bins, number of knots and number of degrees of freedom, is the  
577 one which has proven to deliver good results during the MC based unfolding  
578 procedures discussed before.

579 The comparison of the results, produced with the two analyses, are shown  
580 in Fig. 9. The two spectra show a good agreement, with deviations below  
581 11%.

### 582 *3.1.8. Verification*

583 The shown result which has been obtained with TRUEE has been ver-  
584 ified in terms of the agreement of observable distributions in data and an  
585 accordingly weighted MC event sample. Figure 10 shows the comparison for

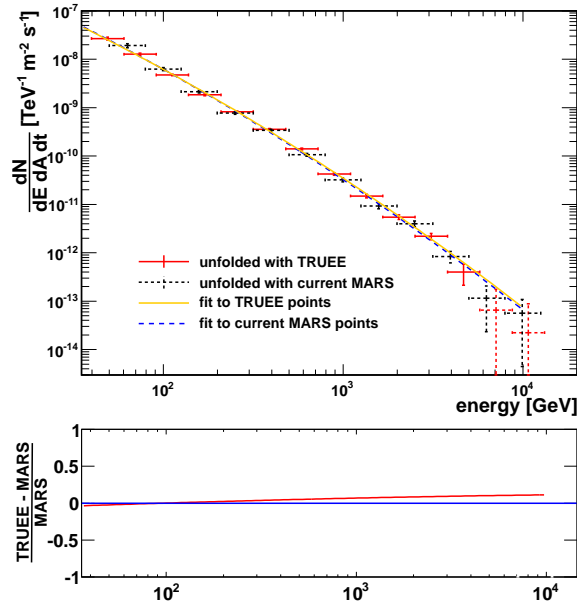


Figure 9: The upper panel presents the unfolded energy spectrum of the Crab Nebula, produced by the example analyses presented here. Shown are results obtained with the current MAGIC unfolding (black/dashed points with error bars) and TRUEE (red/solid points with error bars). Also shown are fits of curved power laws to the unfolded data points. The fit to the standard MARS unfolding is shown in blue/dashed, the fit to TRUEE-unfolded points is depicted in orange/solid. In the bottom panel, the relative deviation of the two fitted functions with respect to the energy is shown.

586 two observables which have been used during the unfolding, while Fig. 11  
 587 displays the distributions for observables which have been neglected during  
 588 the unfolding. Even for observable parameters which have not been consid-  
 589 ered during the unfolding process, the a posteriori distributions match very  
 590 closely. This is a strong confirmation for the quality of the unfolding result.

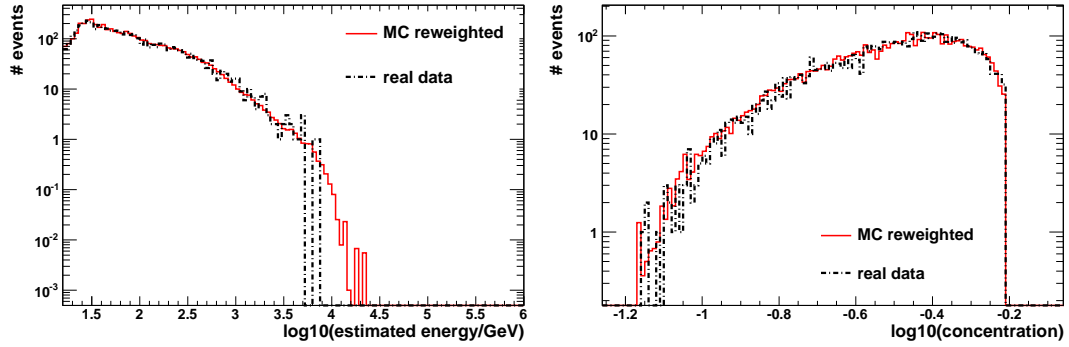


Figure 10: Comparison of distributions in observable parameters which have been used during the unfolding fit. Shown are the estimated energy and concentration distributions for real data (black/dot-dashed) and the re-weighted MC (red/solid).

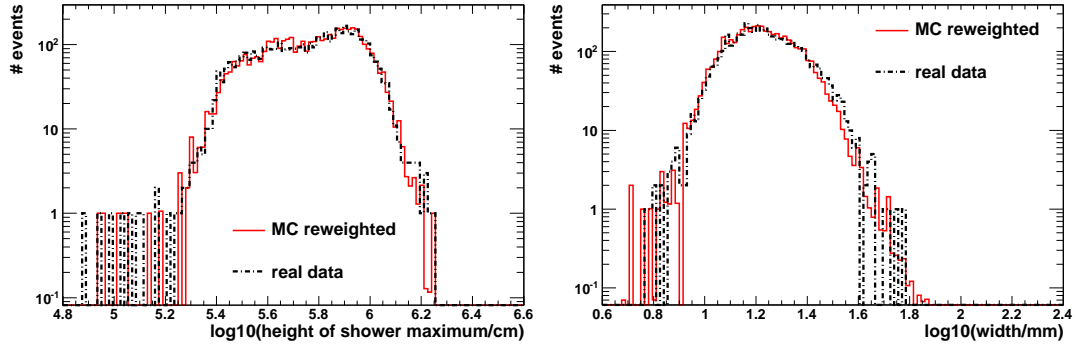


Figure 11: Comparison of observable distributions for real data (black/dot-dashed) and re-weighted MC (red/solid). Shown are observables which have not been considered during the unfolding fit, namely *height of shower maximum* and *width*.

591 *3.2. The IceCube neutrino observatory*

592 *3.2.1. Experiment*

593 IceCube is a cubic kilometer-scale neutrino detector located at the geo-  
594 graphic South Pole. The main goal of IceCube is the investigation of cosmic  
595 rays by the detection of neutrinos. Since neutrinos have a very small in-  
596 teraction cross section and thus pass through a large amount of matter, a  
597 large detection volume is required to obtain neutrino-induced signals with  
598 reasonable statistics. For this reason IceCube utilizes a volume of  $1 \text{ km}^3$   
599 in the glacial ice at the depth between 1 450 and 2 450 m, forming a three-  
600 dimensional grid of 5 160 digital optical modules (DOM) which are equipped  
601 with photomultipliers. The IceCube DOMs are fixed on strings which are  
602 arranged in a triangular pattern in distances of 125 m to each other. The de-  
603 tector deployment has been executed during antarctic summer seasons, from  
604 2005 till 2011. Each year since then, data has been taken with an  $n$ -string  
605 configuration of the partially constructed detector. For the analysis shown  
606 here the IceCube 59 string configuration (IC 59) is used.

607 Neutrinos only undergo weak interaction and thus cannot be detected di-  
608 rectly. They produce secondary particles, such as muons, electrons or tauons  
609 according to the neutrino flavor. These and other secondary charged parti-  
610 cles induce Cherenkov light in the ice if their energy is high enough. The  
611 Cherenkov light propagates through the ice and causes signals, so-called hits,  
612 in the DOMs along the track of the secondary particle within the detector  
613 volume. From the time difference and the amount of charge in each DOM,  
614 the track of the secondary lepton can be reconstructed and its observable  
615 values are saved as one event. Only muons have a track-like signature in

616 the detector and provide sufficient directional information. Therefore, we  
617 consider muon neutrinos in the following.

618 Muons produced in the Earth's atmosphere represent the main component  
619 of the background. In contrast, neutrinos can pass through the Earth, due to  
620 their small cross section. Thus, the Earth can be used as a filter to reduce the  
621 muon background by considering events coming only from below the horizon.

622 In this example analysis the interest is focussed on the determination of  
623 the flux of muon neutrinos coming from decays of charged pions and kaons  
624 that are in turn produced by interactions of cosmic rays with the Earth's  
625 atmosphere. Studying the spectrum of this atmospheric neutrino flux at  
626 energies beyond  $\sim 3 \cdot 10^{14}$  eV can provide information about the production  
627 of charmed mesons in the atmosphere by showing an enhanced neutrino flux  
628 at higher energies, compared to the neutrino flux caused by light meson  
629 decays. Furthermore, a flattening of the neutrino energy spectrum to higher  
630 energies can permit conclusions about the existence of extragalactic high  
631 energy neutrinos, as their predicted flux shows a harder spectral index than  
632 the atmospheric neutrino flux. This would reveal new insights concerning  
633 the different models of cosmic ray production in the cosmic accelerators, such  
634 as Active Galactic Nuclei and Gamma Ray Bursts. Therefore an accurate  
635 estimation of the energy spectrum is essential.

636 In the following, the steps of the regularized unfolding of the neutrino  
637 energy spectrum with TRUEE are demonstrated, by using Monte Carlo sim-  
638 ulations and 10 % of the measured IC 59 data. This analysis serves as a proof  
639 of principle and is not supposed to point out any conclusions about neutrino  
640 physics.

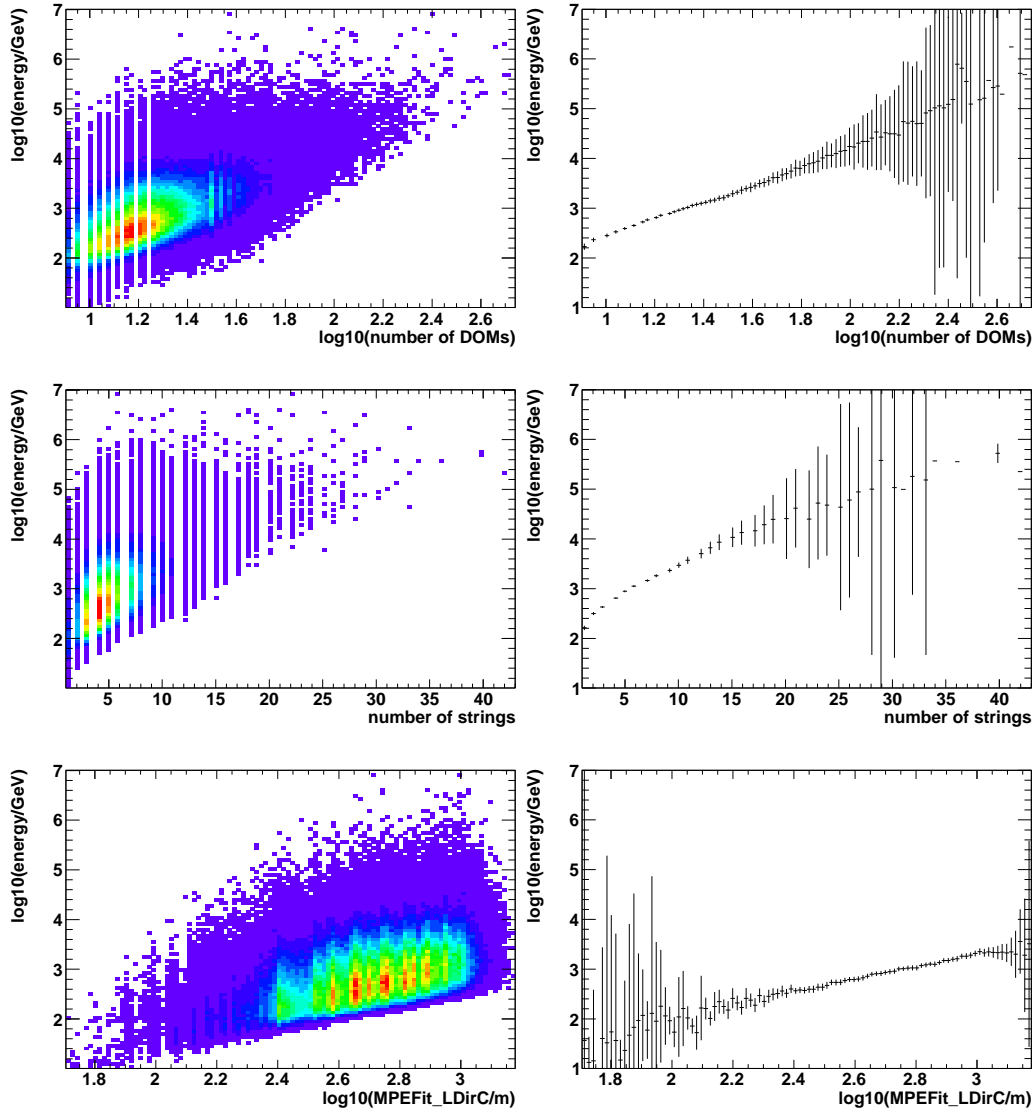


Figure 12: Scatter plots (left) and related profile histograms (right) used to check the correlation between the energy and the observables.

641 *3.2.2. Neutrino sample*

642 For the analysis of the entire neutrino flux a neutrino sample with high pu-  
643 rity is desirable. The background contamination caused by mis-reconstructed  
644 atmospheric muons is chosen not to exceed 5% to keep the uncertainty of  
645 the estimated energy spectrum small compared to statistical uncertainties.  
646 In the following, we use a neutrino sample which was obtained in the course of  
647 the atmospheric neutrino analysis. To reduce the background and to obtain  
648 a neutrino sample with a sufficiently large number of events, series of straight  
649 cuts were applied to the data, including the zenith angle cut  $\theta = 88^\circ - 180^\circ$ .  
650 Although the rejection of muon tracks from above the horizon is made, there  
651 are still mis-reconstructed background events. Therefore the final event se-  
652 lection was performed using the multivariate method Random Forest in the  
653 framework RapidMiner [23]. The final sample consists of  $\sim 3\,000$  events in  
654 the used 10% in the full data sample collected in one year. The correspond-  
655 ing MC sample, which is needed for the event selection training and the  
656 further determination of the response matrix during the unfolding, is pro-  
657 duced using the simulation of all physical processes following the theoretical  
658 models for cross sections and propagations of particles and photons through  
659 different kinds of media. The MC neutrino sample consists of more than  
660  $6 \cdot 10^5$  events, which are weighted to describe the measured data observables  
661 as accurately as possible [24]. Using event weights, the MC energy spectrum  
662 follows the atmospheric neutrino flux with a spectral index  $\gamma \sim 3.7$  predicted  
663 by Honda [25], including the contribution of prompt neutrinos from charm  
664 meson decays at higher energies (Naumov [26]). The simulated background  
665 muon sample, which is used to estimate the purity of the data sample, was

666 produced using the air shower simulator CORSIKA.

### 667 3.2.3. Choice of observables

668 As a first step, the selection of energy-dependent observables is done.  
669 The inspection of the scatter and profile histograms led to the choice of the  
670 following three observables.

- 671 • *Number of DOMs* which show at least one photoelectron. A muon  
672 with higher energy induces more Cherenkov light and has a higher  
673 track length and thus a higher probability to cause hits in DOMs.
- 674 • *Number of strings* which contain at least one hit DOM. This observable  
675 provides additional directional information since the number of strings  
676 is correlated to the zenith angle of the track. Furthermore, the distances  
677 between DOMs on the same string are lower than between those on  
678 different strings. Thus, this observable is supplemental to the number  
679 of DOMs.
- 680 • The direct track length of the muon in a certain time window (*MPE-*  
681 *Fit\_LDirC*). The length is calculated by the projection of the number  
682 of the direct (not scattered) photons on the reconstructed track as the  
683 distance between the two outermost points.

684 The correlation and profile histograms in Fig. 12 show the dependency be-  
685 tween the observables and the energy. In the TRUEE test mode, different  
686 binning of the three observables have been tried in order to find the optimal  
687 unfolding result with respect to the true distribution.

688 *3.2.4. Results*

689 The best result obtained in test mode is shown in Fig. 13. The parameter  
 690 set which delivered the resulting spectrum consisting of 10 bins is given by  
 691 16 knots and 5 degrees of freedom. This combination of parameters is also  
 applied to the real data.

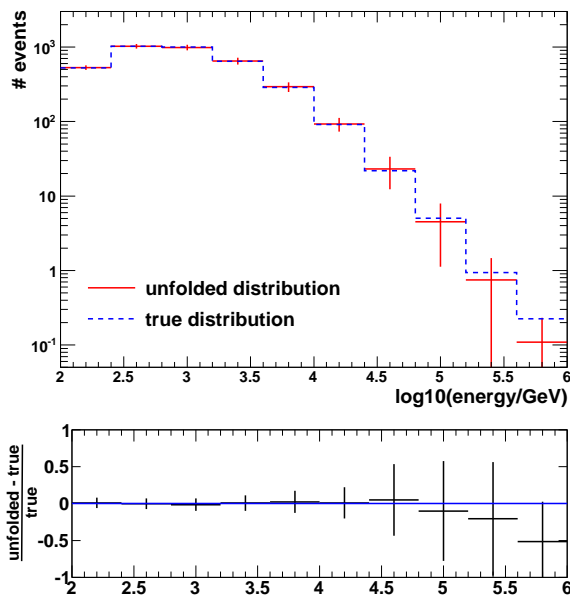


Figure 13: Test mode result for the final unfolding settings. Shown are the true and the unfolded distribution of the part of the MC sample used for the determination of the response matrix. No acceptance correction is applied. The relative difference between the unfolded and true values is shown in the lower histogram.

692

693 The generated MC neutrino sample which is used to determine the de-  
 694 tector response contains only simulated events which undergo an interaction  
 695 within or close to the detector. This restriction is necessary to reduce sim-  
 696 ulation time and memory. Therefore the generated function (here following  
 697  $\sim E^{-2}$ ) does not consider events, which do not cause any signal in the detec-

698 tor, and cannot be given to the unfolding algorithm to normalize the flux to  
 699 the correct scale. However, since we use the individual event weights for the  
 700 MC simulated neutrino sample to make it similar to the real data sample,  
 701 the reweighted sample follows the atmospheric neutrino flux, calculated by  
 702 Honda and Naumov. Thus this atmospheric neutrino flux function can be  
 703 provided to TRUEE to describe the generated neutrino event distribution  
 704 and make the full acceptance correction. We compare this method to the  
 705 standard IceCube analysis procedure using the effective area to scale the fi-  
 706 nal result to the original neutrino flux [27]. This method is described in the  
 707 following.

708 After passing all event selection steps, the final sample contains only  
 709 a fraction of neutrino events. Thus, the unfolded distribution represents  
 710 only neutrinos which interacted, triggered the detector and passed the event  
 selection (Fig. 14).

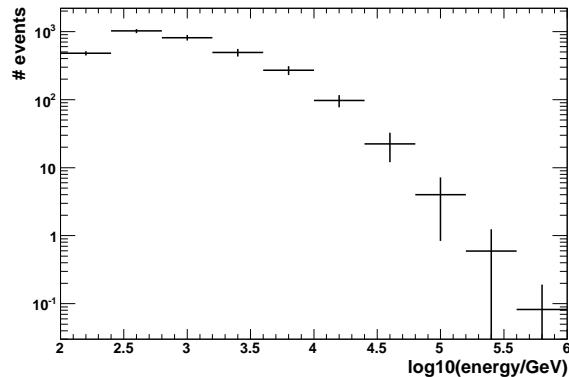


Figure 14: The unfolding of the IC 59 neutrino sample gives the distribution of selected neutrino events depending on energy.

711

712 To calculate the neutrino flux for all neutrinos within the zenith angle

713 range, the unfolded spectrum has to be scaled with the effective area. This is  
 714 the ratio between the observed event rate and the incoming flux and depends  
 715 on the properties of the selected event sample and on the energy. It includes  
 716 the muon neutrino cross section, the probability for the muon to be detected  
 717 and the detector efficiency for muon detection and event reconstruction. The  
 effective area for the current sample is shown in Fig. 15. It rises at higher

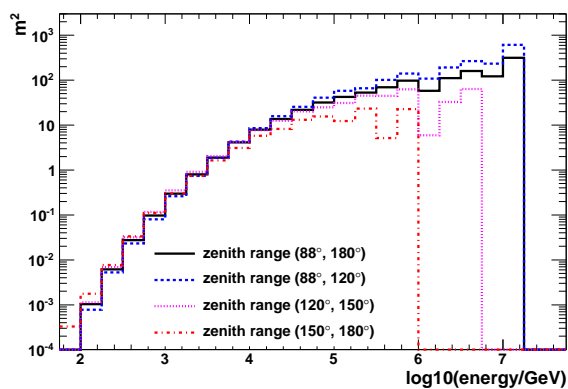


Figure 15: Effective area for the current neutrino sample dependent on neutrino energy. Illustrated are areas for different zenith angle ranges and for the average of the whole zenith range of  $88^\circ$  to  $180^\circ$ , which is considered in the analysis.

718

719 energies due to the increasing cross section of neutrinos and the longer tracks  
 720 of neutrino-induced muons. For the events with vertically upgoing tracks the  
 721 effective area decreases because of the rising probability for absorption of  
 722 neutrinos within the Earth.

723 In Fig. 16, an example of a neutrino flux spectrum is shown, which can  
 724 be derived from an unfolded energy distribution of neutrino events (Fig. 14),  
 725 if the effective area (Fig. 15) is known. Additionally, we present the result  
 726 which has been obtained with the internal acceptance correction by providing

the function of the atmospheric neutrino flux to TRUEE (see also Fig. 16).

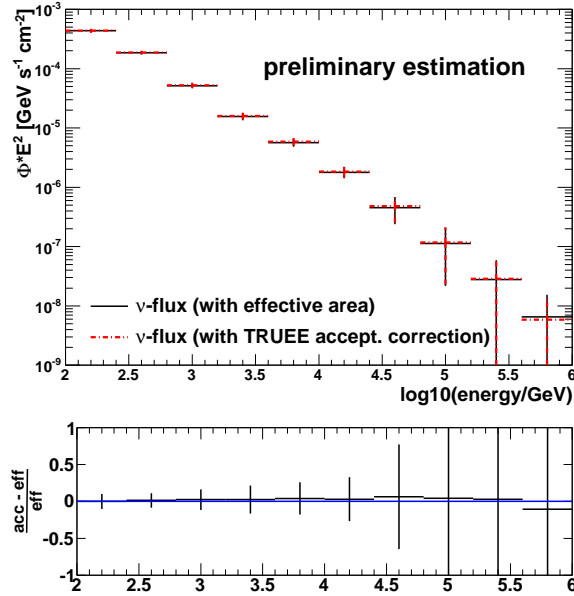


Figure 16: Examples of an atmospheric neutrino energy spectrum gained from 10% of IC 59 data unfolded with TRUEE. The two spectra are obtained using different methods of acceptance correction: the standard IceCube method using effective area (black/solid) and the TRUEE internal acceptance correction (red/dot-dashed). The uncertainties are determined by the unfolding software using standard error propagation, while systematics are not considered in these results. The spectra are weighted with the square of the energy. The relative difference between both distributions is demonstrated in the lower histogram.

727

### 728 3.2.5. Verification

729 To check the quality of the unfolding the agreement between the real data  
 730 and the weighted Monte Carlo sample is investigated. Verification histograms  
 731 of two observables which have not been used for the unfolding fit are shown  
 732 in Fig. 17 and Fig. 18.

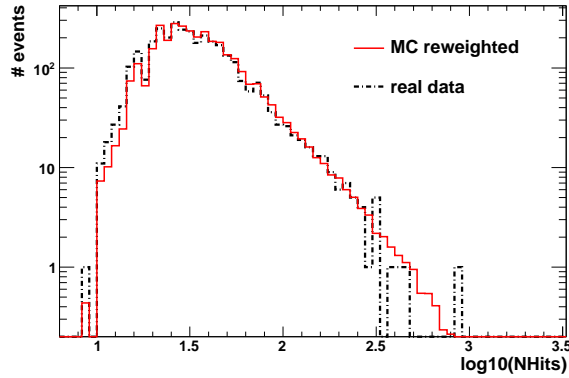


Figure 17: Comparison of data (black/dot-dashed) and MC (red/solid) weighted to the unfolded function. Shown is the number of hits detected in all DOMs per event.

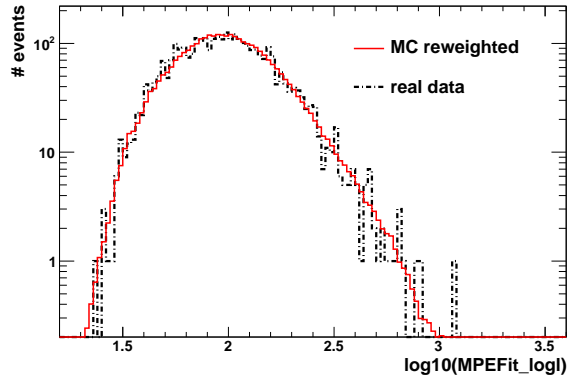


Figure 18: Comparison of data (black/dot-dashed) and MC (red/solid) weighted to the unfolded function. Shown is the log-Likelihood value of an event reconstruction fit.

733 *3.3. Tests on the influence of the simulation*

734 Generally, the unfolding permits the estimation of an unknown distribu-  
 735 tion. With the determined response matrix, the unfolding should be able to  
 736 identify any distribution in the data, independent from the distribution of  
 737 the simulations which have been used for the determination of the response  
 738 matrix. The only requirements are that the simulation model describes the

739 data well enough and that all bins of the observables are filled with a suffi-  
740 cient number of MC events. In general a ten times larger number of simulated  
741 events compared to data events is enough to neglect the uncertainties in the  
742 response matrix [28].

743 In some cases the unfolded distribution can have a very steep spectral  
744 slope. This is also true for astroparticle problems. To ensure that enough  
745 MC events are contained in the high energy region, the spectral slope of  
746 the simulated distribution should not deviate too much from the true data  
747 distribution. The following tests are made to investigate the impact of the de-  
748 viation in the spectral distributions between the MC sample and the pseudo  
749 data sample by using different spectral slopes in the simulation. We use dif-  
750 ferent toy MC samples for the calculation of the response matrix and unfold-  
751 ing which describe the following distributions with respect to the arbitrary  
752 variable  $x$

- 753 • power law with  $\gamma = 3.7$  (related to the atmospheric neutrino flux)
- 754 • power law with  $\gamma = 3.5$
- 755 • power law with  $\gamma = 3.0$
- 756 • power law with  $\gamma = 2.5$ .

757 The different MC simulations which are used for the determination of the  
758 response matrix are shown in Fig. 19.

759 We present unfolding results of two pseudo data samples with the steepest  
760 ( $\gamma = 3.7$ ) and the flattest ( $\gamma = 2.5$ ) power law. The results are shown in  
761 Fig. 20 and Fig. 21. The slope of the pseudo data sample is the same or

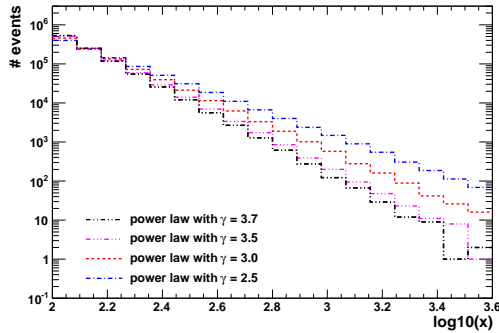


Figure 19: Four toy MC samples used for the determination of the individual response matrices. The simulated distributions have different spectral slopes.

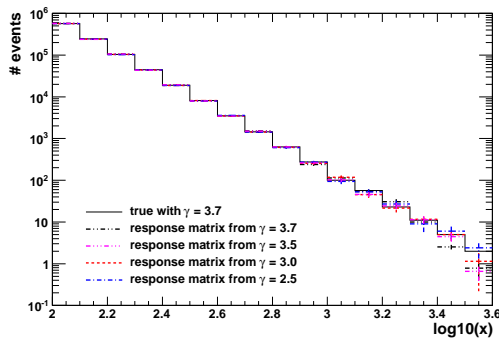


Figure 20: Unfolding results of the simulated pseudo data sample following the power law with  $\gamma = 3.7$  using different MC simulated distributions for the response matrix calculation. The true sought distribution is shown by the solid line.

762 steeper than the slope of the MC samples. The maximum deviation between  
 763 the spectral indices of MC and pseudo-data is 1.2. The unfolding results  
 764 with the flatter MC assumptions are consistent with the true distribution  
 765 within the uncertainties. The MC sample with the steepest spectral slope  
 766 causes an underestimation of the event distribution at x-values greater than  
 767  $\log_{10}(x) = 3.4$ . This is caused by the fact that the response matrix is not  
 768 well enough described due to the low amount of events. Instead, the x-region

769 below  $\log_{10}(x) = 3.4$  has bins containing more than 10 events and thus a  
 770 good agreement of the unfolded result with the true distribution is ensured.  
 771 The same is true for the unfolding of the power law distribution with  $\gamma = 2.5$ .

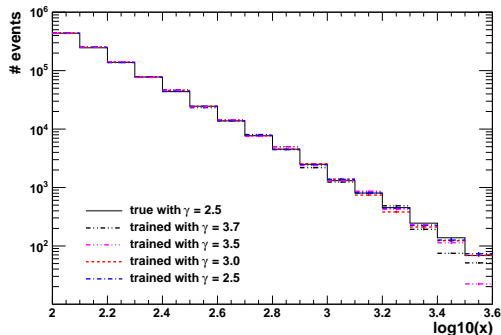


Figure 21: Unfolding results of the simulated pseudo data sample following the power law with  $\gamma = 2.5$  using different MC simulated distributions for the response matrix calculation. The true sought distribution is shown by the solid line.

772 The conclusion of the test is the recommendation to use a MC sample  
 773 for the response matrix which features a similar or harder spectrum com-  
 774 pared to the real data, especially if the unfolded distribution covers several  
 775 orders of magnitude. The bins of the MC sought distribution should contain  
 776 at least 10 events. In case of a completely unknown true distribution, an  
 777 iterative approach of matching the MC spectral slope to the real data can be  
 778 executed.

#### 779 4. Summary and outlook

780 The new unfolding software TRUEE has been tested within the astropar-  
 781 ticle experiments MAGIC and IceCube and appears to be a very suitable tool  
 782 for astroparticle physics, since it can properly estimate distributions which

783 cover several orders of magnitude. The input of all samples is event-wise,  
784 thus the response matrix is calculated with an individual binning for every  
785 distinct case. A moderate deviation of the distribution of simulated events,  
786 used to determine the response matrix, from the data distribution is tolera-  
787 ble, thus an a-priori knowledge of the exact spectral slope of the estimated  
788 distribution is not necessary.

789 In TRUEE, the uncertainties are calculated in the same way as was done  
790 in *RUN*. They have been proven to follow the Poisson distribution or, in  
791 the case of a large number of events, the Gaussian distribution [29]. There-  
792 fore the exclusion of values outside the uncertainties can be made with the  
793 minimal probability of 68%. An additional investigation to calculate con-  
794 fidence intervals is being developed within the collaborative research center  
795 SFB 823. Within the same project the time dependency of TRUEE will be  
796 implemented. Instead of time-slices, the unfolding will be able to deliver a  
797 two-dimensional distribution. This is suggested by the fact that a simple  
798 fragmentation of the data sample in several packages along the time axis is  
799 unacceptable to get reasonable results in cases of low statistics.

800 Furthermore, an option which allows to automatically perform a sec-  
801 ond unfolding iteration with a re-weighted MC sample will be implemented.  
802 Thereby potentially large differences in the spectral distributions in MC and  
803 data can be avoided, which is especially important for the case of an accep-  
804 tance correction within TRUEE. While the procedure itself has been pre-  
805 sented and verified here, only its integration into the program is still to be  
806 performed.

807 TRUEE has been developed in the programming language C++. It

808 contains the proven algorithm  $\mathcal{RUN}$  and additional user-friendly functions,  
809 which offer a more comfortable handling of an unfolding analysis. The soft-  
810 ware is easy to install and convenient to use in combination with modern  
811 software. TRUEE and the original algorithm  $\mathcal{RUN}$  deliver comparable re-  
812 sults.

813 TRUEE is intended to be included in the common framework for unfold-  
814 ing software RooUnfold [30]. Additionally, TRUEE is currently tested by  
815 several particle physics groups.

816 Within the collaborative research center SFB 823, the fields of application  
817 of the program TRUEE will be expanded to solving problems in the context  
818 of economics and engineering.

819 The TRUEE software and the user manual can be found at [http://app.tu-  
820 dortmund.de/TRUEE/](http://app.tu-dortmund.de/TRUEE/).

## 821 **Acknowledgment**

822 This research is supported by the DFG through the Collaborative Re-  
823 search Center SFB 823, project C4 and the DAAD PPP-Spanien program,  
824 which are gratefully acknowledged. We acknowledge the support from the  
825 collaborations of the experiments MAGIC and IceCube. Special thanks are  
826 directed to the members of the “Statistics Tools Group” of the Helmholtz  
827 Alliance “Physics At The Terascale” for productive discussions. We would  
828 also like to thank Julian Krause for helpful discussions on the MAGIC data  
829 analysis.

830 [1] V. Blobel, Unfolding methods in high energy physics experiments,  
831 CERN Yellow Report 85-02 (1985).

- 832 [2] E. Fredholm, Sur une classe d'équations fonctionnelles, *Acta Math.* 27  
833 (1903) 365–390.
- 834 [3] C. de Boor, *A Practical Guide to Splines*, Springer, 2001.
- 835 [4] A. Tikhonov, On the solution of ill-posed problems and the method of  
836 regularization, *Dokl. Akad. Nauk SSSR* 151 (1963) 501 – 504.
- 837 [5] V. Blobel, E. Lohrmann, *Statistische und numerische Methoden der*  
838 *Datenanalyse*, Teubner, 1998.
- 839 [6] V. Blobel, The RUN manual: regularized unfolding for high-energy  
840 physics experiments., *OPAL Technical Note TN361* (1996).
- 841 [7] K. Martin, W. Hoffman, *The CMake Build Manager - Cross platform*  
842 *and open source*, Dr. Dobbs (2003).
- 843 [8] I. Chakravarti, R. Laha, J. Roy, *Handbook of Methods of Applied Statis-*  
844 *tics*, volume 1, John Wiley and Sons, 1967.
- 845 [9] E. Carmona, et al., Performance of the MAGIC Stereo System, *Proc.*  
846 *32nd ICRC, Beijing, China* (2011).
- 847 [10] F. Halzen, S. R. Klein, *IceCube: An Instrument for Neutrino Astron-*  
848 *omy*, *Rev.Sci.Instrum.* 81 (2010) 081101.
- 849 [11] R. K. Bock, et al., Methods for multidimensional event classifica-  
850 tion: a case study using images from a Cherenkov gamma-ray telescope,  
851 *Nucl.Instrum.Meth.* A516 (2004) 511–528.

- 852 [12] T. Voigt, et al., Threshold Optimization for Classification in Imbal-  
853 anced Data with Unknown Misclassification Costs (2011). Submitted to  
854 Advances in Data Analysis and Classification.
- 855 [13] J. Albert, et al., Implementation of the Random Forest  
856 Method for the Imaging Atmospheric Cherenkov Telescope MAGIC,  
857 Nucl.Instrum.Meth. A588 (2008) 424–432.
- 858 [14] V. P. Fomin, et al., New methods of atmospheric Cherenkov imaging  
859 for gamma-ray astronomy. I. The false source method, Astroparticle  
860 Physics 2 (1994) 137–150.
- 861 [15] A. Moralejo, et al., MARS, the MAGIC Analysis and Reconstruction  
862 Software, arXiv:0907.0943 (2009).
- 863 [16] A. M. Hillas, Cerenkov light images of EAS produced by primary  
864 gamma, Proc. 19th ICRC, San Diego, California (1985) 445–448.
- 865 [17] L. Breiman, Random Forests, Machine Learning 45 (2001) 5–32.
- 866 [18] D. Heck, et al., CORSIKA: A Monte Carlo code to simulate extensive  
867 air showers, Wissenschaftliche Berichte FZKA 6019 (1998).
- 868 [19] E. Carmona, et al., Monte Carlo Simulation for the MAGIC-II System,  
869 Proc. 30th ICRC, Merida, Yucatan, Mexico (2007) 1373–1376.
- 870 [20] J. Albert, et al., Unfolding of differential energy spectra in the MAGIC  
871 experiment, Nucl.Instrum.Meth. A583 (2007) 494–506.

- 872 [21] M. Bertero, Linear inverse and ill posed problems, *Advances in Electron-*  
873 *ics and Electron Physics*, ed. P.W.Hawkes 75 (1989) 1–120. INFN/TC-  
874 88/2.
- 875 [22] M. Schmelling, The Method of reduced cross entropy: A General ap-  
876 proach to unfold probability distributions, *Nucl.Instrum.Meth. A340*  
877 (1994) 400–412.
- 878 [23] S. Fischer, et al., Yale: Yet Another Learning Environment, Techni-  
879 cal Report CI-136/02, Collaborative Research Center 531, University of  
880 Dortmund, 2002. ISSN 1433-3325. <http://yale.sf.net/> .
- 881 [24] T. Montaruli, F. Ronga, Comparison of muon and neutrino times from  
882 decays of mesons in the atmosphere, arXiv:1109.6238 (2011).
- 883 [25] M. Honda, et al., Calculation of atmospheric neutrino flux using the  
884 interaction model calibrated with atmospheric muon data, *Phys.Rev.*  
885 *D75* (2007) 043006.
- 886 [26] E. Bugaev, et al., Prompt Leptons in Cosmic Rays, *Il Nuovo Cimento*  
887 *12 C* (1989).
- 888 [27] R. Abbasi, et al., Measurement of the atmospheric neutrino energy  
889 spectrum from 100 GeV to 400 TeV with IceCube, *Phys.Rev. D83*  
890 (2011) 012001.
- 891 [28] V. Blobel, An Unfolding method for high-energy physics experiments,  
892 *Contributions to the Conference on Advanced Statistical Techniques in*  
893 *Particle Physics*, Durham (2002) 258–267.

- 894 [29] K. Muenich, Messung des atmosphärischen Neutrinospektrums mit  
895 dem AMANDA-II Detektor, Dissertation (2007).
- 896 [30] T. Auye, Unfolding algorithms and tests using RooUnfold,  
897 arXiv:1105.1160 (2011).